Research Article | Vol. 30, No. 24 / 21 Nov 2022 / Optics Express 43223
Optics EXPRESS

# Photonically-driven Schottky diode based 0.3 THz heterodyne receiver

Iñigo Belio-Apaolaza,[1,*] James Seddon,[1] Diego Moro-Melgar,[2] Hanu Priya Indiran,[1] Chris Graham,[1] Katarzyna Balakier,[1] Oleg Cojocari,[2] and Cyril C. Renaud[1]

[1]Department of Electronic and Electrical Engineering, University College London, London WC1E 7JE, UK
[2]ACST GmbH, Josef-Bautz-Str. 15, 63457 Hanau, Germany
[*]inigo.apaolaza.21@ucl.ac.uk

**Abstract:** Photonics-based technologies are key players in a number of emerging applications in the terahertz (THz) field. These solutions exploit the well-known advantages of optical devices, such as ultra-wide tuneability and direct integration with fiber networks. However, THz receivers are mainly implemented by fully electronic solutions, where Schottky barrier diodes (SBD) are the preferred option as detectors and mixers due to their excellent response within the THz range at room temperature, and technological maturity. Here, we demonstrate an SBD-based subharmonic mixer (SHM) at 300 GHz pumped with a photonic local oscillator. The Schottky mixer is a prototype designed and manufactured by *ACST GmbH*, operating at 270-320 GHz. The local oscillator is generated by photomixing on a high-frequency and high-power uni-travelling-carrier photodiode (UTC-PD), providing enough power to saturate conversion loss. Minimum single-side-band conversion loss of 14.4 dB and a peak dynamic range of 130 dB have been measured. Finally, as a proof of concept we realize an all-photonics-based 5 Gbps wireless bridge, utilizing the optically-pumped SBD mixer. With this work, we prove the feasibility of high-performance hybrid Schottky-photonic THz receivers, incorporating the best of both worlds.



## 1. Introduction

The terahertz (THz) frequency electromagnetic band can be defined from 0.1 THz to 30 THz [1], filling the gap between infrared light and microwave radiation. Historically, radio-astronomy has driven the development of THz technologies, but in the last few decades, a variety of applications have attracted great interest, including telecommunications [2,3], material science [4,5], biological and biomedical sciences [6–8], and security imaging [9–11] among others.

In this context of emerging trends, photonics-based THz technologies are playing an important role in the generation, detection, processing and transportation of THz signals, constituting the so-called field of THz photonics [12,13]. Optical devices and techniques are particularly attractive for THz applications because they offer intrinsic advantages such as ultra-wide tuneability and low-loss fiber propagation. In THz communications for example, links enabled by high-frequency and high-power uni-travelling-carrier photodiodes (UTC-PD) are among the systems with the highest data rates achieving over 100 Gbps [14,15]. In addition, photonics-based solutions can be directly integrated with fiber networks, where mature coherent technology can be exploited, thus implementing seamless THz-fiber systems.

The receiver side of THz systems is currently dominated by all-electronic solutions [16,17]. A wide range of THz receivers are based on heterodyne detection, down-converting to a much lower intermediate-frequency (IF), by mixing the THz wave with a reference signal, which is often denoted as local oscillator (LO). This scheme has been used for decades in microwave and THz systems, with well-known advantages such as an improvement in sensitivity, frequency

#471102 https://doi.org/10.1364/OE.471102
Journal © 2022 Received 28 Jul 2022; revised 10 Oct 2022; accepted 10 Oct 2022; published 9 Nov 2022

Optics EXPRESS

channel selection, IF amplification and processing, and coherent detection. Some types of THz mixers include superconductor-insulator-superconductor (SIS) mixers [18,19], hot electron bolometers (HEB) [20,21], field effect transistors (FETs) [22,23], and optoelectronic mixers based on low-temperature-grown GaAs/InGaAs (LTG-GaAs/InGaAs) photoconductors [24–26], and UTC-PDs [27].

All of these present particular advantages and limitations. SISs and HEBs exhibit the lowest noise equivalent power (NEP) and require low LO power (~1-100 uW), but SISs must operate at cryogenic temperatures (~ 4K), and although HEBs are capable of room temperature operation, cryogenic cooling is required to obtain low NEP. FETs are a promising semiconductor solution for uncooled detectors, but they still face challenges regarding THz wave coupling and integration with other components. Optoelectronic mixers incorporate the advantages of photonics but the reported conversion efficiencies and IF bandwidths are lower than other THz mixer technologies.

Additionally, planar GaAs Schottky barrier diode (SBD) mixers have been the leading solution as THz heterodyne receivers especially for space applications, due to their characteristics of high conversion efficiency, low parasitics, low weight and compactness, high IF bandwidth, and room temperature operation [28,29]. Nowadays, commercial THz Schottky mixers are widely available, being a more mature and reliable option than other competing technologies. One of the main drawbacks of these mixers is that the required LO power is typically above 0 dBm, which limits the use of photomixers as LO signal generators.

In photonic local oscillator systems, the generation can be decentralized and distributed over a fiber-network [30]. By exploiting the ultra-wide tuneability of photonic sources, the same LO unit can be used to cover multiple THz bands. Furthermore, the resulting phase noise does not suffer from a penalty associated with typically used electronic LO multiplier chains, where the phase noise is increased by $20log(N)$, with N as the factor of multiplication. Thus, with phase-locked optical sources, comparable or even lower phase noise can be achieved [31,32]. These features make this approach particularly attractive for applications such as wireless communication networks or radio-astronomy. In fact, radio observatories like LMSA and ALMA already implement photonic LO systems, but only serving as a reference signal [33] or pumping SIS mixers [34,35], with the aforementioned limitations.

This work presents the first successful THz Schottky mixer at 300 GHz pumped with a photonic local oscillator, generated by photomixing in an UTC-PD. The key feature of the Schottky mixer is the implementation of low-barrier InGaAs-based diodes, significantly reducing the required LO power. The first section of the paper is devoted to the description of the receiver. Characterization methods and results are contained in sections 3 and 4 respectively. Finally, we demonstrate the receiver in a real-world application, by realizing a THz wireless bridge between two optical ends, enabled by photonics both at the transmitter and the receiver.

## 2. 270-320 GHz SBD mixer and UTC-PD receiver

The schematic of the optically pumped receiver is depicted in Fig. 1(a). The subharmonic mixer (SHM) operates within the band 270-320 GHz and the local oscillator signal must be provided at half the RF band, i.e. 135-160 GHz. The down-converted IF signal can be varied from 0 to 18 GHz. The RF, LO and IF ports are based on rectangular waveguide WR-3.4, WR-6.5, and an SMA connector respectively. A pyramidal antenna is used to couple the incoming RF signal. The SHM implements low-barrier SBDs on an antiparallel configuration (Fig. 1(b)), suppressing odd harmonic mixing products [36]. The resulting IF is related to the RF and LO frequencies by $f_{IF} = f_{RF} - 2f_{LO}$.

The low-barrier SBDs are based on a InGaAs compound in combination with particular metals to realize the Schottky junction [37]. The resulting barrier height lies within 0.2-0.3 eV, compared to typical ~0.8 eV of GaAs SBDs. This enables zero-bias operation with low power

Optics EXPRESS

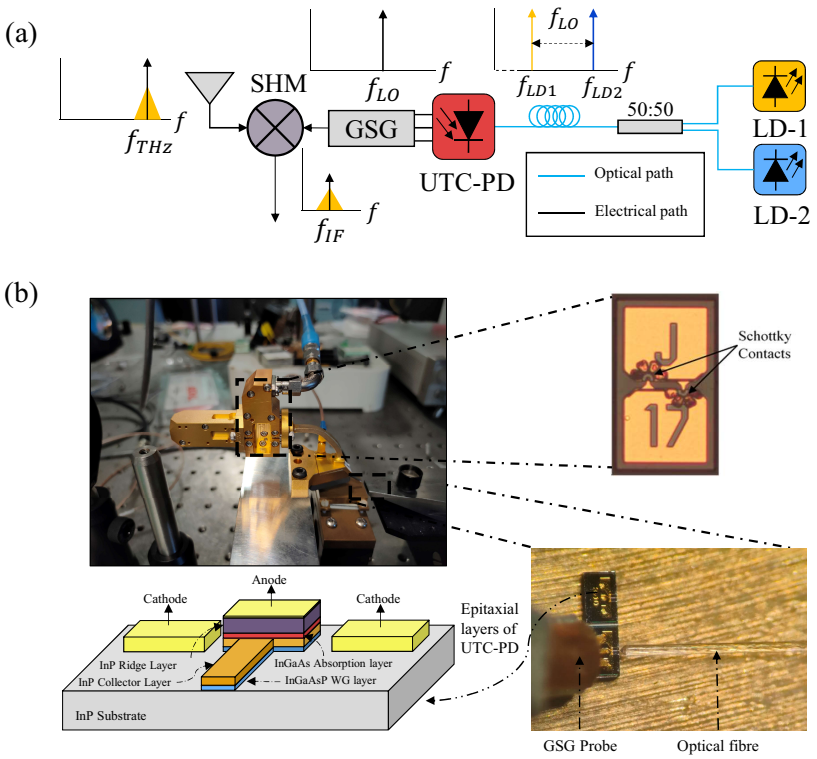


**Fig. 1.** Schottky mixer and photonic local oscillator receiver: (a) Schematic of the receiver. The local oscillator signal is generated by optical heterodyning on an UTC-PD at the first even harmonic of the incoming RF signal. (b) Physical arrangement and component insights of the receiver.

LO requirements. The Schottky diodes and the mixer have been fully designed and fabricated at ACST GmbH, employing a proprietary Film-Diode (FD) technology process [38].

A waveguide-integrated UTC-PD with 3x10 $\mu m^2$ of active area integrated with a co-planar waveguide generates the LO signal at the 135-160 GHz band acting as a photomixer. In this type of photodiode, a thin p-type quasi-neutral layer of InGaAs is used as an absorber [39]. The photo-generated majority holes respond within the relaxation time, which is as low as 33 fs for lattice-matched InGaAs [40]. Therefore, only electrons contribute to the UTC-PD response, for which the drift velocity in InGaAs can be up to 10 times higher than for holes. This also contributes to the reduction of the space-charge effect in the depletion layer, resulting in a higher output saturation power [39]. The particular epitaxial layers, structure, and fabrication details of the UTC-PD used in this work can be found in [41].

Two 1.55 $\mu m$ free-running lasers with emitting frequencies $f_1$ and $f_2$ separated by the desired LO frequency $f_{LO}$ pump the UTC-PD. Light is coupled horizontally to the photodiode waveguide via an optical fiber, as shown in Fig. 1(b). An optical heterodyning process [42] on the UTC-PD generates an electrical signal of frequency $f_{LO}$ at the output. In order to couple the output of UTC-PD with the LO port, we use a GSG probe as shown in Fig. 1(b). The probe is a Cascade Microtech air co-planar (ACP) WR-8 model with 90-140 GHz of bandwidth, which incorporates a bias T allowing the DC voltage of the UTC-PD to be set. Notice that the rectangular waveguide size does not match the LO input port, and the cut-off frequency is lower than the maximum required LO frequency. This inevitably results in lower power delivered to the mixer's Schottky

Optics EXPRESS

diodes. However, as shown later, the power is enough to drive the mixer at optimum conditions across most of the operating band.

## 3. Characterization setups and methods

### 3.1. Radio-frequency and local oscillator power measurements

The first step to characterize the receiver is to measure the incoming RF and LO power. The setup for this purpose is depicted in Fig. 2. The THz transmitter used in this study is based on an antenna-integrated (bow-tie type) UTC-PD photomixer, fabricated and packaged at UCL [43]. The UTC-PD package includes an aplanetic hyper hemispherical silicon lens of 6 mm diameter, used to shape the radiated THz beam.

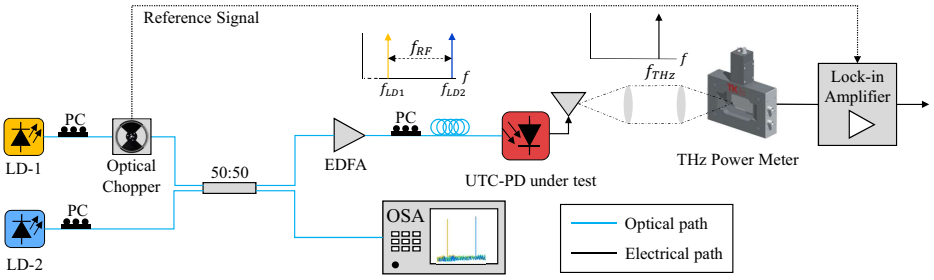


**Fig. 2.** Schematic of the RF and LO power measurement setup using a Thomas Keating power meter. PC: Polarization controller, LD: Laser diode, OSA: Optical spectrum analyzer, EDFA: Erbium-doped fiber amplifier.

The power of the radiated wave is detected by a Thomas Keating absolute power meter, based on the opto-acoustic effect. Two 1.55 $\mu m$ continuous-wave (CW) lasers, one fixed at 1553.73 nm (RIO Orion Series) and one tuneable (Agilent 81682A), generate two optical waves separated by the desired THz frequency $f_{THz}$. The tuneable laser signal is chopped at a frequency of 15 Hz, and the reference chopping signal is sent to a lock-in amplifier connected to the output of the power detector. An Erbium-doped fiber amplifier (EDFA) (Thorlabs EDFA100S) is placed before the transmitter to compensate for optical losses and maximize the input power to the UTC-PD. The optical power of each signal at the input of the EDFA was 3.5 dBm and 2 dBm for the UTC-PD THz transmitter and the UTC-PD LO generator respectively. A set of 3 polarization controllers (PC) ensure that both laser signals' polarizations are aligned between them and with respect to the photodiode's optical waveguide mode.

The radiated THz wave propagates across a 20 cm free-space path, which includes two Polytetrafluoroethylene (PTFE) lenses (Thorlabs PTFE LAT075) and an infrared (IR) block (Tydex LPF8.8-35). In order to determine and calibrate the laser frequency separation, a high-resolution (10 MHz) optical spectrum analyzer (OSA) is employed (BOSA Aragon Photonics). When measuring the LO power, the output of the GSG probe is coupled to a WR-8 Flann 20 dB standard gain horn antenna. In this case, the THz power meter is placed at a very close distance (2 cm) from the antenna, to ensure all the emitted power is collected by the power meter.

The RF and LO powers are measured from 220 GHz to 320 GHz in 0.5 GHz steps, and from 135 GHz to 160 GHz in 0.25 GHz steps, respectively. For each point, the frequency of the tuneable laser is set and calibrated according to the fixed laser frequency measured at the OSA. After 10 seconds of settling time, the power is measured by storing a 1-minute-long trace from the lock-in amplifier (time constant of 10 seconds) for each frequency. The optical power at the input of the UTC-PD THz transmitter was 20 dBm, generating a photocurrent of 9.2 mA when biased at −2 V, whereas for the UTC-PD LO generator, the optical power was set to 18.4 dBm resulting in 15 mA of photocurrent when biased at −3 V.

Optics EXPRESS

### 3.2. Schottky mixer characterization

Once the RF and LO powers have been measured, the characterization of the Schottky mixer's performance is carried out, which consists of a set of IF power measurements. The schematic of the setup for this purpose is depicted in Fig. 3. In this case, an additional laser (Agilent 81640A) is required to generate a signal with a frequency separation $f_{LO}$ from the fixed laser. The same fixed laser is used to generate both the RF and LO frequencies, by incorporating two-by-two 50:50 couplers in an arrangement as shown in Fig. 3. The three laser signals are also combined and connected to the OSA, enabling calibration and measurement of their frequency separation.

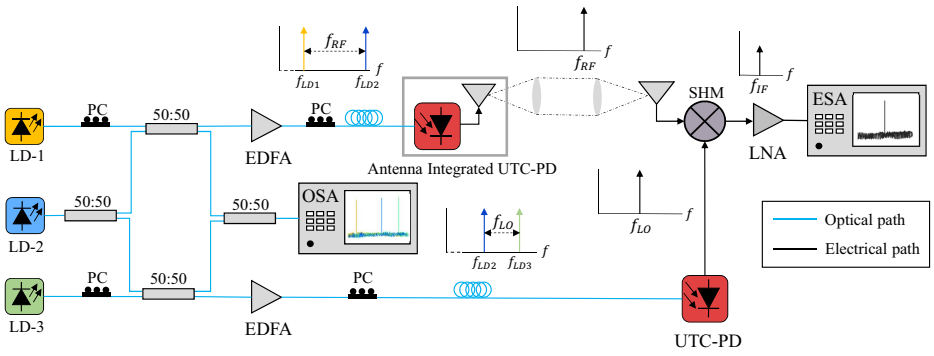


**Fig. 3.** Schematic of the sub-harmonic mixer characterization setup. LNA: low noise amplifier, SHM: Sub-harmonic mixer, ESA: Electrical spectrum analyzer. PC: Polarization controller, LD: Laser diode, OSA: Optical spectrum analyzer, EDFA: Erbium-doped fiber amplifier.

The free-space path from the transmitter to the SHM antenna is the same as in the RF power measurement setup to ensure that the power levels at the input of the SHM are equal in both cases. The 20 cm distance ensures that the SHM's antenna is operating in far-field conditions. To verify that no significant near-field effects are added by using the PTFE lenses, we additionally measured the received power varying the distance between the two lenses between 5 cm and 100 cm, measuring always the same power with a ± 0.5 dB difference. The same optical powers at the input of the EDFAs as in the previous setup are set, biasing the UTC-PD transmitter again at −2 V. A low-noise amplifier (LNA) with a frequency range of 0.01 to 30 GHz and 40 dB typical gain (RF-Lambda RLNA00G30GA), is connected at the output of the SHM to raise the power level of the down-converted IF signal. The output of the LNA is connected to an R&S FSU-26 electrical spectrum analyzer (ESA) where we measure the IF power.

With this setup, several figures of merits (FoMs) were measured. In particular, single-side-band conversion loss (SSB-CL), IF response, sensitivity, and dynamic range. SSB-CL is the most important FoM of an electronic mixer, because it determines the efficiency of the frequency conversion. It is defined as the ratio between the input RF power and output IF power, and in this case it is calculated as follows

$$SSB_{CL}(dB) = P_{RF}(dBm) - P_{IF}(dBm) + G_{IF}(dB) \tag{1}$$

where $P_{RF}$ is the RF power measured previously, $P_{IF}$ is the IF power measured at the ESA, and $G_{IF}$ is the IF path gain, including the LNA and all cables and connectors. $P_{IF}$ for the SSB-CL characterization was measured by setting −3 V of bias voltage and 15 mA of photocurrent (18.4 dBm of optical input power) at the UTC-PD LO generator. The SSB-CL was obtained from 270 to 320 GHz of RF frequency in 0.5 GHz steps, tuning the lasers accordingly to have a constant IF frequency of 1 GHz. For each frequency point, 10 values of IF power, RF, LO and IF frequencies are recorded, with 8 seconds of settling time between points. The gain of the full IF path from

Optics EXPRESS

0.01 to 30 GHz is obtained with a calibrated measurement on a vector network analyzer (VNA). In addition to that, SSB-CL was measured by varying the optical input power of the UTC-PD LO generator, i.e. at different photocurrents and incoming RF frequencies. This measurement allows us to determine that the UTC-PD provides enough LO power to reach the optimum operating point of the Schottky mixer, saturating the received IF power, and therefore the SSB-CL. The input optical power is increased from −1.5dBm to 18.4 dBm in 0.2 dB steps, resulting in a photocurrent ranging from 0.1 to 15 mA. This was repeated for several frequencies from 270 to 320 GHz and bias voltages of −1, −2, and −3 V.

The IF response shows the IF power decay from low to higher frequencies, giving the 3 dB IF bandwidth of the Schottky mixer. To measure this FoM, the RF frequency is fixed at 270 GHz, setting the LO frequency for an initial IF of 0.5 GHz. The LO is tuned accordingly to measure power from 0.5 to 20.5 GHz. The IF response is obtained by normalizing with respect to the power at 0.5 GHz and the IF path gain.

Finally, we measured sensitivity and dynamic range. In this study we define the sensitivity as the noise power density observed at the ESA, normalized to 1 Hz of bandwidth, i.e. the minimum detectable IF signal power. This is carried out using the same procedure as for SSB-CL, but turning the THz transmitter off, and measuring the noise power density at the ESA, across the RF band of the Schottky mixer. Once the sensitivity is measured, the dynamic range is obtained by the ratio of the sensitivity to the maximum power measured for each RF frequency. Notice that the sensitivity is limited by the full receiver system, including noise contributions of the IF components and instruments, and not only by the electronic mixer's NEP. The dynamic range in this case is also limited by the radiated power of the THz transmitter.

## 4. Characterization results

### 4.1. Radio-frequency and local oscillator power

The measured RF power is depicted in Fig. 4(a). Shaded error bars represent a confidence interval of $\pm\sigma$ in every plot of the presented results. A maximum power of −17.44 dBm was measured at 220 GHz and a minimum power of −25.61 dBm at 320 GHz. The standard deviation is typically less than 1 dB. Characterizing RF power with low error is critical because it will accumulate for SSB-CL.

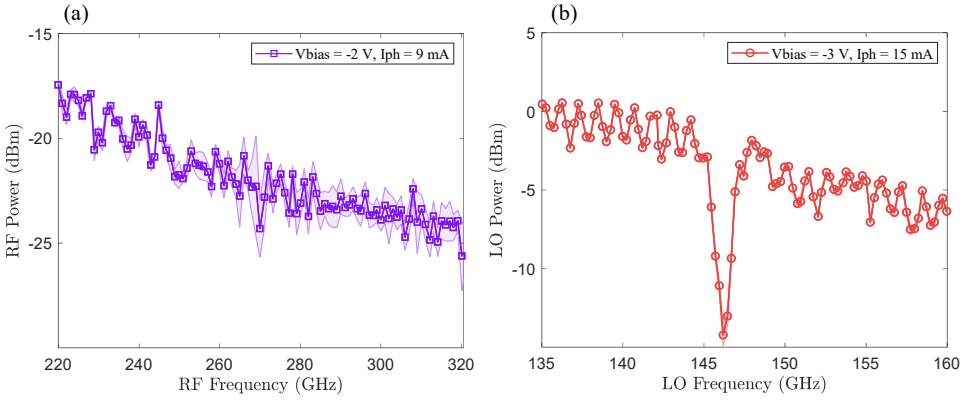


**Fig. 4.** Power measurement results: (a) Transmitted RF power from the antenna-integrated UTC-PD from 220 to 320 GHz. Reverse bias voltage is set to 2 V, giving a photocurrent of 9.2 mA. (b) LO power generated by the GSG probed UTC-PD, from 135 to 160 GHz. Reverse bias voltage is set to 3 V, giving a photocurrent of 15 mA.

Optics EXPRESS

Figure 4(b) shows the measured LO power. In this case, error bars are barely visible. This is attributed to the fact that the LO power is much higher than the noise equivalent power of the Thomas Keating Power meter, estimated at 1 uW (−30 dBm). A maximum power of 0.53 dBm is measured at 136.25 GHz and a minimum of −14.23 dBm at 146.25 GHz, where a resonant feature can be observed. This behaviour can be attributed to the WR-8 probe, as it is rated up to 140 GHz and the cut-off frequency of the rectangular waveguide upper mode is expected to be at 147.5 GHz, being fairly close to the measured resonance. The second minimum of −7.51 dBm is measured at 157.75 GHz. The overall power decay is caused by a combination of UTC-PD frequency response and ACP probe bandwidth. As the Schottky mixer is designed to require a LO power of approximately −7 dBm, low powers at higher LO frequencies will have an impact on conversion loss, as shown in the next subsection. Another feature of the measured IF power is the considerable ripple with a period of approximately 1 GHz. This is attributed to the impedance mismatch between the probe, which expects a load of 50 Ω, and the UTC-PD, which has a complex value with a real part of ∼ 5-10 Ω [43,44].

### 4.2. Conversion loss and intermediate-frequency response

Figure 5 depicts the results of the SSB-CL measurement increasing UTC-PD LO generator photocurrent for multiple frequencies and bias voltages. There are several factors that play a role, but we can mainly identify: (1) LO power generated by the UTC-PD, (2) SHM conversion loss saturation, and (3) effective LO power coupled to the Schottky diodes. All of these factors influence the results, and their particular contribution is dependent on the frequency of operation. Conducting the measurements with different bias conditions, together with the previously discussed LO power measurement (Fig. 4(b)), allows us to extract a solid interpretation of the results of Fig. 5.

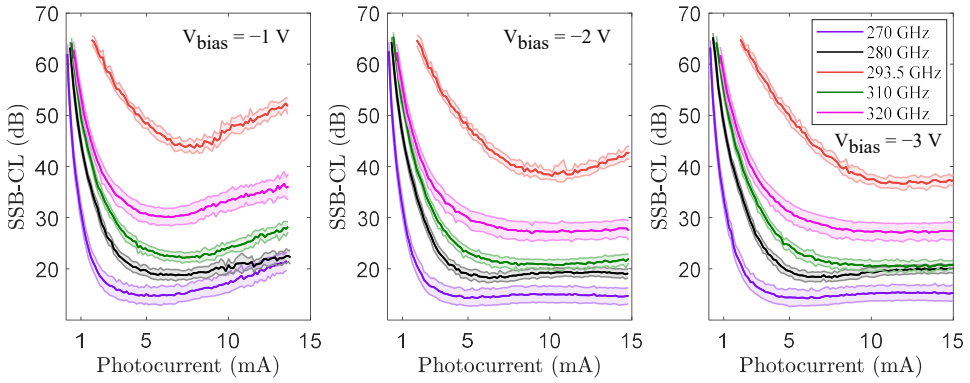


**Fig. 5.** SSB-CL (measured at 1 GHz of IF) versus photocurrent at the UTC-PD LO generator at different frequencies and bias voltage. Optical input power is varied from −1.51 to 18.4 dBm, resulting on a photocurrent from 0.1 to 15 mA.

Output electrical current and input optical power in a photodiode are related linearly until saturation is reached. For higher bias voltages we expect to observe saturation occurring at higher photocurrent [43,45]. The 293.5 GHz case is especially interesting because it coincides with an LO frequency of 146.25 GHz, where the dip feature aforementioned is present. The LO power at that frequency at optimal conditions is significantly lower than the required power to drive the Schottky mixer. Therefore, the curves of 293.5 GHz indicate the point of UTC-PD output power saturation. Considering this, we observe that for −1 V and −2 V conversion loss is minimized at a photocurrent of 7.93 mA and 10.13 mA respectively. At −3 V, power is clearly saturated, but a

Optics EXPRESS

significant decay is not observed yet at 15 mA. These observations match previously reported results on UTC-PD power saturation with this particular structure [41].

That being said, curves corresponding to −2 V and −3 V clearly demonstrate conversion loss saturation, reaching the operational point of the Schottky mixer. This occurs for a photocurrent as low as 4.8 mA (13 dBm of optical power) for 270 GHz, obtaining a minimum SSB-CL of 14.4 dB. As the RF frequency is increased, saturation is reached at higher photocurrent. This follows the LO power decrease trend for increasing LO frequencies shown in Fig. 4(b). At 320 GHz SSB-CL is significantly lower than the other saturated cases. This can be attributed to a power decay in the RF path, probably due to the antenna bandwidth. For 270 GHz and 280 GHz, we can observe that the SSB-CL is minimized and then increases slightly for higher photocurrent, while UTC-PD power is still not saturated. One can expect to observe this on a Schottky mixer when the LO power is higher than the optimum. In contrast, for the 310 and 320 GHz cases, the power is enough to reach the optimum operation point but not to detriment the SSB-CL.

The obtained SSB-CL for the full operating range of the Schottky mixer taken on a separate measurement is depicted in Fig. 6. The typical value is below 20 dB for most of the frequency range, showing a relatively flat response with the 293.5 GHz peak discussed. The 3 dB IF bandwidth of the Schottky mixer has been measured at 19.5 GHz (Fig. 7), again exhibiting a relatively flat response. The IF bandwidth is set by design, and it is mainly limited because of the SMA connector.

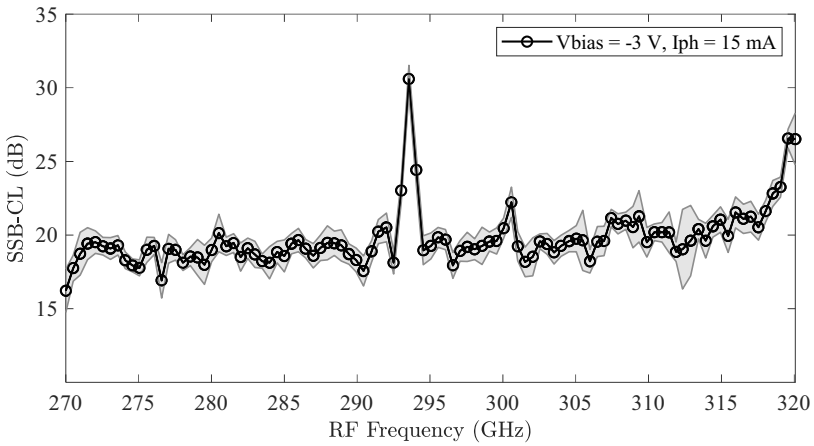


**Fig. 6.** SSB-CL from 270 to 320 GHz measured at 1 GHz of IF. The reverse bias voltage of the UTC-PD LO generator is set at −3V with an input optical power of 18 dBm resulting in 15 mA of photocurrent.

These results show that even for LO frequencies above 146.25GHz, where LO power is of the order of −6 dBm, the Schottky mixer still operates at optimum conditions. Dual-side-band conversion loss (DSB-CL) reported on state-of-the-art GaAs Schottky sub-harmonic mixers at this frequency band is of the order of ∼7 dB [46–48]. Considering that DSB-CL is ideally 3 dB lower than SSB-CL, and the ∼15-20 dB of SSB-CL reported here, there is a ∼ 5-10 dB difference. However, LO power required to drive GaAs SBD mixers is about 10 dB higher than this work, which is a significant difference. In addition, the design of the SHM for this fabrication run has not been fully optimized. Future design and fabrication iterations could potentially improve SSB-CL to state-of-the-art Schottky performance. Compared to optoelectronic LTG-GaAs mixers, a minimum conversion loss of ∼ 27 dB has been reported [25], which is about one order of magnitude higher than the conversion loss shown here. The same comparison applies for UTC-PDs as optically pumped mixers, with 30 dB conversion loss at the 300 GHz band [27].

Optics EXPRESS

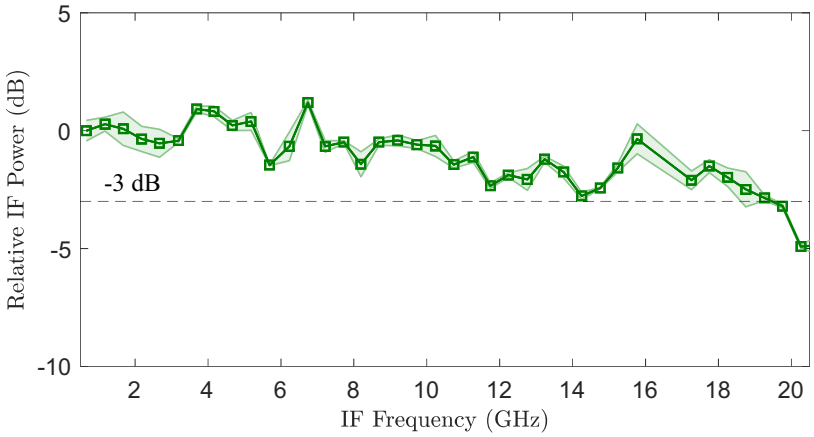


**Fig. 7.** IF response from 0.5 to 20 GHz. The RF frequency is fixed at 270 GHz and the LO is varied from 134.75 to 144.75 GHz.

### 4.3. *Sensitivity and dynamic range*

Figure 8(a) shows the measured noise power density. The receiver's noise has a contribution from the ambient, Schottky mixer, LO, cables, LNA, and ESA noise. First, a noise power density of −130 dBm/Hz was measured with the LO signal off, isolating noise not coming from the Schottky mixer. For greater photocurrent, i.e. higher LO power, the noise power density increases, and the trend follows the same as the LO power discussed previously. This indicates that the sensitivity in this case is limited by the contribution from the LO, but only by less than 3 dB compared to the LO off scenario. The ripple at lower photocurrent is more significant because the power is not enough to saturate conversion loss across the whole band.

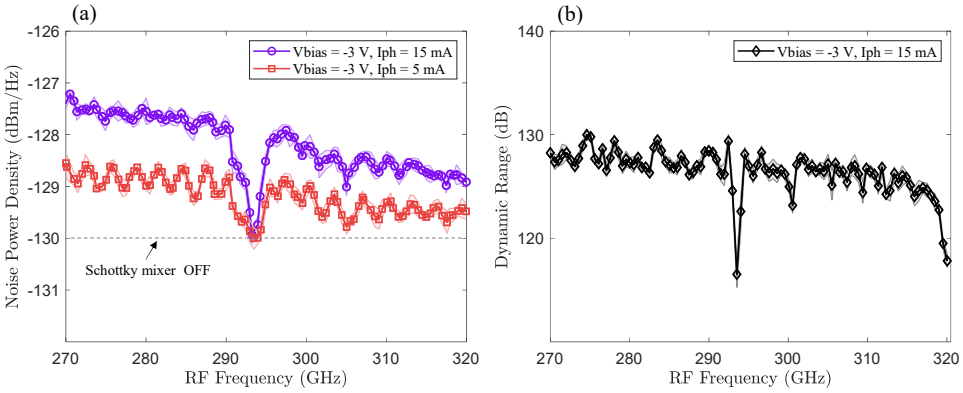


**Fig. 8.** Sensitivity and dynamic range measurements: (a) Obtained noise power density from 270 to 320 GHz. (b) Measured dynamic range from 270 to 320 GHz, normalized to 1 Hz of bandwidth.

Dynamic range as high as 130 dB (normalized to 1 Hz of bandwidth) has been measured (Fig. 8(b)). This FoM is particularly relevant for spectroscopy applications. To put our obtained values into context, maximum dynamic ranges of ~110 dB have been reported in the literature using InGaAs-based photoconductors in CW THz spectroscopy systems [49–51]. These systems typically rely on lock-in amplification, and therefore the dynamic range can be normalized considering $\tau_c = 1/2\pi f$, where $\tau_c$ is the time constant set in the lock-in amplifier and $f$ is the

Optics EXPRESS

equivalent 3 dB bandwidth. For 1 Hz bandwidth, the equivalent time constant is approximately 160 ms. That gives a normalized literature-reported record of 109 dB [51]. Our system demonstrates a 20 dB improvement in comparison, setting a new record. It is important to remark that the systems to which we are comparing are ultra-wide (over 1 THz of bandwidth), whereas our THz system is limited by the 50 GHz bandwidth of the SHM. Nevertheless, our results show the potential of this particular type of receiver to realize high-performance THz spectroscopy systems.

A simple way to improve the sensitivity and dynamic range of the receiver would be to include a band-pass optical filter to cancel out-of-band LO noise, which is mainly amplified spontaneous emission (ASE) noise coming from the EDFA. The LNA has a typical noise figure of 4 dB, so selecting a better IF amplifier would also improve the receiver's noise. It is important to remark that both sensitivity and dynamic range are FoMs that evaluate the performance of the whole receiver, and not only the optically driven mixer. In addition, the dynamic range has been obtained by considering the THz power generated by the UTC-PD transmitter as maximum. Using a better packaged device would also improve this FoM.

## 5. 5 Gbps all-photonics-based wireless bridge at 270 GHz

In this section, we demonstrate an application of the proposed receiver in the context of data communications. As proof of concept, a transparent wireless bridge between two optical ends operating at 5 Gbps was implemented. This type of communication system is expected to play a role in future 6G networks, connecting seamlessly multiple ends of the network at high speeds, reducing the bottleneck of current wireless links in mobile networks by exploiting THz communications [14,52].

The schematic of the implemented link is depicted in Fig. 9(a). The transmitter and receiver are very similar to the ones used for characterization with the differences specified here. In the transmitter, one of the lasers is intensity modulated by a Mach-Zehnder modulator (MZM), which is driven with a 5 Gbps baseband signal coming from a Pseudorandom bit sequence (PRBS) generator. The radiated THz wave propagates across the same path used for characterization, and it is down-converted to 10 GHz of IF frequency with the photonically driven SHM. Then, a chain of 2 LNAs (RF-Lambda RLNA00G30GA) raises the IF power to optimal levels to drive a second MZM to up-convert the IF signal into the optical domain, modulating an additional laser at 1554.8 nm (Rio Orion Series). The optical wave is filtered to generate a suppressed-carrier single-side-band modulation (SC-SSB). This step is necessary to perform a non-coherent optical detection as the lasers are not frequency or phase-locked. Then, the optical signal is amplified with an EDFA before reaching the optoelectronic receiver, which is based on a 50 GHz bandwidth pin photodiode (Finisar XPDV2120R) connected to a high-frequency oscilloscope (Teledyne LeCroy LabMaster 10-36Zi). Note that LD-1 and LD-3 depicted in the schematic are indeed the same laser at 1553.7 nm (Rio Orion Series), following the arrangement of Fig. 3. Two tuneable lasers (Agilent 81682A and Agilent 81640A) are required for this experiment, represented as LD-2 and LD-4 in the schematic. For simplicity, the fiber segments are only a few meters long, but several kilometres of fiber length are feasible thanks to the ultra-low propagation losses and chromatic dispersion immunity due to the SC-SSB modulation.

The eye diagram depicted in Fig. 9(d) was captured in real-time for over 300 seconds, exhibiting error-free detection. Previously reported THz wireless bridges implement receivers relying on electronically-driven mixers [53–55] or direct THz-to-Optical conversion using ultra-wide bandwidth plasmonic modulators [56,57]. The first approach's drawbacks are related to the generation of the LO signal, adding complexity and power consumption to the THz front-ends. In contrast, in our proposed solution the LO signal can be distributed over a fiber network, relocating and centralizing complexity and power consumption where it can be handled more easily. The second approach, although very efficient, lacks the ability to perform channel selection and IF

Optics EXPRESS

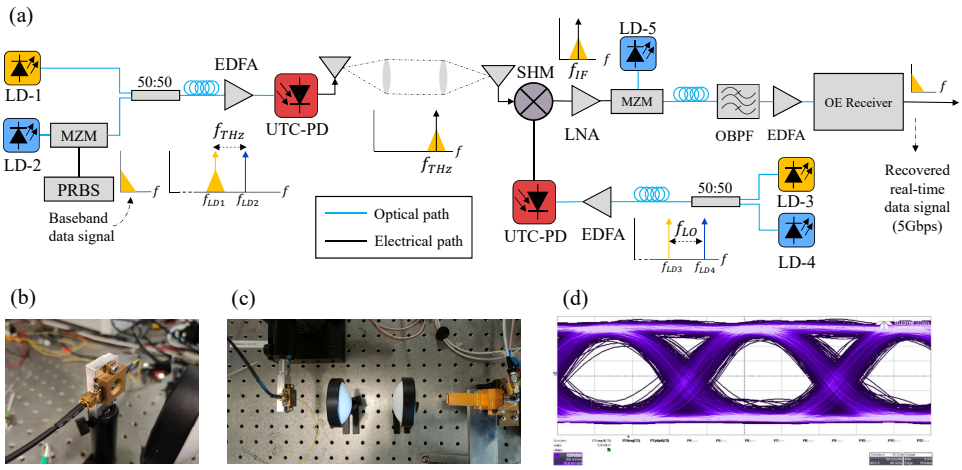


**Fig. 9.** Optical-THz-Optical bridge at 270 GHz: (a) Schematic of the experiment (polarization controllers are omitted). (b) Packaged antenna-integrated UTC-PD used for characterization as THz transmitter. (c) THz free-space path with the optically pumped mixer at the receiver end. (d) Eye diagram obtained with a capturing time of over 5 minutes. LNA: low noise amplifier, SHM: Sub-harmonic mixer, ESA: Electrical spectrum analyzer. PC: Polarization controller, LD: Laser diode, OSA: Optical spectrum analyzer, EDFA: Erbium-doped fiber amplifier. PRBS: Pseudo-random bit sequence generator, MZM: Mach-Zehnder modulator, OBPF: Optical band-pass filter, OE: Optoelectronic.

processing before upconverting again into the optical domain, which may be desirable in future generation networks. Thus, our solution enables simultaneously efficient down-conversion and photonic LO generation and distribution. It should be noticed that this experiment represents a basic demonstration employing the presented receiver, and there is great room for optimization. By selecting better lasers, using complex modulation formats, and exploiting the full IF bandwidth of the Schottky mixer, we can expect to transmit at rates of 100 Gbps over longer distances.

## 6. Conclusion

In summary we have presented, to the best of the authors' knowledge, the first demonstration of a 300 GHz Schottky-based SHM pumped with an UTC-PD that demonstrates enough LO power to saturate conversion loss. The Schottky mixer exhibits single-side-band conversion losses on the order of ~ 15-20 dB across the RF band, 19.5 GHz of IF bandwidth, and a peak dynamic range of 130 dB when using the mixer in a receiver system. These values outperform previously reported THz optoelectronic mixers, although the conversion loss is higher than state-of-the-art Schottky mixers. The results of this study indicate that the SHM operates in saturation even with a gross LO power of −7 dBm. Our claim of having enough LO power generated by the UTC-PD is reinforced by considering that we show saturation even at frequencies that are 20 GHz beyond the bandwidth of the ACP probe. In addition, optimization of impedance matching between LO port and UTC-PD has not been considered in this study. Addressing this issue would also improve the performance, allowing us to realize higher frequency receivers. Finally, we have demonstrated the optically pumped receiver in a real-world application, realizing an Optical-THz-Optical bridge at 5 Gbps, thus highlighting the applicability of such receivers.

With this work, we demonstrate the potential of hybrid Schottky UTC-PD THz receivers, featuring high-performance THz heterodyne detection and mature Schottky technology combined with the advantages of optically generated LO signals. This is a first step toward the practical realization of these receivers, which can be used in a wide number of applications outperforming

Optics EXPRESS

other solutions. Future work should be focused on the integration of the Schottky mixer and UTC-PD, investigating the possibility of hybrid and monolithic on-chip solutions. By integrating the SBDs and the UTC-PD in the same chip, LO power coupling and bandwidth could be improved compared to rectangular waveguide access. Similarly, the RF bandwidth could be improved by implementing a quasi-optical solution.

**Funding.** Horizon 2020 Framework Programme TERAPOD (761579); Horizon 2020 Marie Skodowska-Curie Actions TERAOPTICS (956857).

**Acknowledgments.** The authors would like to acknowledge Alexis Bernini for his help in setting up the experiments.

**Disclosures.** The authors declare no conflicts of interest.

**Data availability.** Data underlying the results presented in this paper are not publicly available at this time but may be obtained from the authors upon reasonable request.

## References

1. S. Dhillon, M. Vitiello, and E. Linfield, *et al.*, "The 2017 terahertz science and technology roadmap," J. Phys. D: Appl. Phys. **50**(4), 043001 (2017).
2. T. Kleine-Ostmann and T. Nagatsuma, "A review on terahertz communications research," J. Infrared, Millimeter, Terahertz Waves **32**(2), 143–171 (2011).
3. Z. Chen, X. Ma, B. Zhang, Y. Zhang, Z. Niu, N. Kuang, W. Chen, L. Li, and S. Li, "A survey on terahertz communications," China Commun. **16**(9), 1–14 (2019).
4. F. Ospald, W. Zouathi, R. Beigang, C. Matheis, J. Jonuscheit, B. Recur, J.-P. Guillet, P. Mounaix, W. Vleugels, P. Venegas Bosom, L. Vega Gonzalez, I. Lopez, R. Martinez Edo, Y. Sternberg, and M. Vandewal, "Aeronautics composite material inspection with a terahertz time-domain spectroscopy system," Opt. Eng. **53**(3), 031208 (2013).
5. M. Y. Glyavin, G. G. Denisov, V. E. Zapevalov, M. A. Koshelev, M. Y. Tretyakov, and A. I. Tsvetkov, "High-power terahertz sources for spectroscopy and material diagnostics," Phys.-Usp. **59**(6), 595–604 (2016).
6. J.-H. Son, S. J. Oh, and H. Cheon, "Potential clinical applications of terahertz radiation," J. Appl. Phys. **125**(19), 190901 (2019).
7. A. Gong, Y. Qiu, X. Chen, Z. Zhao, L. Xia, and Y. Shao, "Biomedical applications of terahertz technology," Appl. Spectrosc. Rev. **55**(5), 418–438 (2020).
8. A. G. Markelz and D. M. Mittleman, "Perspective on terahertz applications in bioscience and biotechnology," ACS Photonics **9**(4), 1117–1126 (2022).
9. M. C. Kemp, P. F. Taday, B. E. Cole, J. A. Cluff, A. J. Fitzgerald, and W. R. Tribe, "Security applications of terahertz technology," in *Terahertz for Military and Security Applications*, vol. 5070 R. J. Hwu and D. L. Woolard, eds., International Society for Optics and Photonics (SPIE, 2003), pp. 44–52.
10. H.-B. Liu, H. Zhong, N. Karpowicz, Y. Chen, and X.-C. Zhang, "Terahertz spectroscopy and imaging for defense and security applications," Proc. IEEE **95**(8), 1514–1527 (2007).
11. S. Ergün and S. Sönmez, "Terahertz technology for military applications," J. Mil. Inf. Sci. **3**(1), 13–16 (2015).
12. A. J. Seeds, M. J. Fice, K. Balakier, M. Natrella, O. Mitrofanov, M. Lamponi, M. Chtioui, F. van Dijk, M. Pepper, G. Aeppli, A. G. Davies, P. Dean, E. Linfield, and C. C. Renaud, "Coherent terahertz photonics," Opt. Express **21**(19), 22988–23000 (2013).
13. D. Saeedkia and S. Safavi-Naeini, "Terahertz photonics: Optoelectronic techniques for generation and detection of terahertz waves," J. Lightwave Technol. **26**(15), 2409–2423 (2008).
14. T. Nagatsuma, G. Ducournau, and C. C. Renaud, "Advances in terahertz communications accelerated by photonics," Nat. Photonics **10**(6), 371–379 (2016).
15. T. Kürner, D. Mittleman, and T. Nagatsuma, *THz Communications: Paving the Way Towards Wireless Tbps* (Springer, 2022), pp. 299–309.
16. K. Sengupta, T. Nagatsuma, and D. M. Mittleman, "Terahertz integrated electronic and hybrid electronic–photonic systems," Nat. Electron. **1**(12), 622–635 (2018).
17. Y.-J. Lin and M. Jarrahi, "Heterodyne terahertz detection through electronic and optoelectronic mixers," Rep. Prog. Phys. **83**(6), 066101 (2020).
18. A. Karpov, D. Miller, F. Rice, J. Stern, B. Bumble, H. LeDuc, and J. Zmuidzinas, "Low Noise 1 THz–1.4 THz Mixers Using Nb/Al-AlN/NbTiN SIS Junctions," IEEE Trans. Appl. Supercond. **17**(2), 343–346 (2007).
19. K. H. Gundlach and M. Schicke, "SIS and bolometer mixers for terahertz frequencies," Supercond. Sci. Technol. **13**(12), R171–R187 (2000).
20. W. Zhang, P. Khosropanah, J. Gao, E. L. Kollberg, K. Yngvesson, T. Bansal, R. Barends, and T. Klapwijk, "Quantum noise in a terahertz hot electron bolometer mixer," Appl. Phys. Lett. **96**(11), 111113 (2010).
21. I. Tretyakov, S. Ryabchun, M. Finkel, A. Maslennikova, N. Kaurova, A. Lobastova, B. Voronov, and G. Gol'tsman, "Low noise and wide bandwidth of NbN hot-electron bolometer mixers," Appl. Phys. Lett. **98**(3), 033507 (2011).
22. B. Gershgorin, V. Y. Kachorovskii, Y. Lvov, and M. Shur, "Field effect transistor as heterodyne terahertz detector," Electron. Lett. **44**(17), 1036 (2008).

Optics EXPRESS


23. E. Javadi, D. B. But, K. Ikamas, J. Zdanevičius, W. Knap, and A. Lisauskas, "Sensitivity of field-effect transistor-based terahertz detectors," Sensors **21**(9), 2909 (2021).
24. I. Kostakis, D. Saeedkia, and M. Missous, "Characterization of low-temperature InGaAs-InAlAs semiconductor photo mixers at 1.55 $\mu$m wavelength illumination for terahertz generation and detection," J. Appl. Phys. **111**(10), 103105 (2012).
25. E. Peytavit, F. Pavanello, G. Ducournau, and J.-F. Lampin, "Highly efficient terahertz detection by optical mixing in a GaAs photoconductor," Appl. Phys. Lett. **103**(20), 201107 (2013).
26. S. Hisatake, G. Kitahara, K. Ajito, Y. Fukada, N. Yoshimoto, and T. Nagatsuma, "Phase-Sensitive Terahertz Self-Heterodyne System Based on Photodiode and Low-Temperature-Grown GaAs Photoconductor at 1.55 $\mu$m," IEEE Sens. J. **13**(1), 31–36 (2013).
27. C. C. Renaud, M. Natrella, C. Graham, J. Seddon, F. Van Dijk, and A. J. Seeds, "Antenna integrated THz uni-traveling carrier photodiodes," IEEE J. Sel. Top. Quantum Electron. **24**(2), 1–11 (2018).
28. A. Maestrini, B. Thomas, H. Wang, C. Jung, J. Treuttel, Y. Jin, G. Chattopadhyay, I. Mehdi, and G. Beaudin, "Schottky diode-based terahertz frequency multipliers and mixers," C. R. Phys. **11**(7-8), 480–495 (2010).
29. I. Mehdi, J. V. Siles, C. Lee, and E. Schlecht, "THz diode technology: Status, prospects, and applications," Proc. IEEE **105**(6), 990–1007 (2017).
30. P. Shen, N. J. Gomes, P. A. Davies, W. P. Shillue, P. G. Huggard, and B. N. Ellison, "High-purity millimetre-wave photonic local oscillator generation and delivery," in *MWP 2003 Proceedings. International Topical Meeting on Microwave Photonics, 2003* (IEEE, 2003), pp. 189–192.
31. A. Ueda, T. Noguchi, S. Asayama, H. Iwashita, Y. Sekimoto, M. Ishiguro, H. Ito, T. Nagatsuma, A. Hirata, and W. Shillue, "Ultra-low noise photonic local oscillator at 100 GHz," Jpn. J. Appl. Phys. **42**(Part 2, No. 6B), L704–L705 (2003).
32. E. A. Kittlaus, D. Eliyahu, S. Ganji, S. Williams, A. B. Matsko, K. B. Cooper, and S. Forouhar, "A low-noise photonic heterodyne synthesizer and its application to millimeter-wave radar," Nat. Commun. **12**(1), 4397 (2021).
33. W. Shillue, W. Grammer, C. Jacques, R. Brito, J. Meadows, J. Castro, J. Banda, and Y. Masui, "The ALMA photonic local oscillator system," in *2011 XXXth URSI General Assembly and Scientific Symposium* (IEEE, 2011), pp. 1–4.
34. T. Shuro, A. Ueda, T. Yamamoto, S. Asayama, Y. Sekimoto, T. Noguchi, M. Ishiguro, H. Takara, S. Kawanishi, H. Ito, A. Hirata, and T. Nagatsuma, "The First Radioastronomical Observation with Photonic Local Oscillator," Publ. Astron. Soc. Jpn. **55**(4), L53–L56 (2003).
35. I. C. Mayorga, A. Schmitz, T. Klein, C. Leinz, and R. Gusten, "First in-field application of a full photonic local oscillator to terahertz astronomy," IEEE Trans. Terahertz Sci. Technol. **2**(4), 393–399 (2012).
36. M. Cohn, J. E. Degenford, and B. A. Newman, "Harmonic mixing with an antiparallel diode pair," IEEE Trans. Microwave Theory Tech. **23**(8), 667–673 (1975).
37. I. Oprea, A. Walber, O. Cojocari, H. Gibson, R. Zimmermann, and H. Hartnagel, "183 GHz mixer on InGaAs schottky diodes," 21st Int. Symp. On Space Terahertz Technology, pp. 23–25 (2010).
38. O. Cojocari, I. Oprea, H. Gibson, and A. Walber, "SubMM-wave multipliers by film-diode technology," in *46th European Microwave Conference (EuMC)* (IEEE, 2016), pp. 337–340.
39. H. Ito, S. Kodama, Y. Muramoto, T. Furuta, T. Nagatsuma, and T. Ishibashi, "High-speed and high-output InP-InGaAs unitraveling-carrier photodiodes," IEEE J. Sel. Top. Quantum Electron. **10**(4), 709–727 (2004).
40. T. Ishibashi, S. Kodama, N. S. N. Shimizu, and T. F. T. Furuta, "High-speed response of uni-traveling-carrier photodiodes," Jpn. J. Appl. Phys. **36**(Part 1, No. 10), 6263–6268 (1997).
41. X. Lin, M. Natrella, J. Seddon, C. Graham, C. C. Renaud, M. Tang, J. Wu, H. Liu, and A. J. Seeds, "High performance waveguide uni-travelling carrier photodiode grown by solid source molecular beam epitaxy," Opt. Express **27**(25), 37065–37086 (2019).
42. S. Iezekiel, *Microwave Photonics: Devices and Applications* (John Wiley & Sons, 2009), pp. 88–90.
43. J. P. Seddon, M. Natrella, X. Lin, C. Graham, C. C. Renaud, and A. J. Seeds, "Photodiodes for Terahertz Applications," IEEE J. Sel. Top. Quantum Electron. **28**(2: Optical Detectors), 1–12 (2022).
44. C. Mukherjee, M. Natrella, J. Seddon, C. Graham, P. Mounaix, C. C. Renaud, and C. Maneux, "Efficient compact modelling of UTC-photodiode towards terahertz communication system design," Solid-State Electron. **170**, 107836 (2020).
45. R. S. Quimby, *Photonics and Lasers: An Introduction* (John Wiley & Sons, 2006), Chap. 14.
46. D. Pardo Santos, "Analysis and design of multipliers and mixers via Monte Carlo modelling at THz bands," Ph.D. thesis (Universidad de Salamanca, 2014).
47. Virginia Diodes Inc., "Mixers (SHM, EHM and FM)," https://www.vadiodes.com/en/products/mixers-shm-ehm-and-fm. Accessed: 2022-09-20.
48. ACST GmbH, "Mixers," https://acst.de/products/mm-sub-mm-wave-modules/mixers. Accessed: 2022-09-20.
49. R. B. Kohlhaas, S. Breuer, S. Nellen, L. Liebermeister, M. Schell, M. P. Semtsiv, W. T. Masselink, and B. Globisch, "Terahertz time-domain spectroscopy system using rhodium doped InGaAs antennas: 637 $\mu$W peak power and 110 dB dynamic range," in *45th International Conference on Infrared, Millimeter, and Terahertz Waves (IRMMW-THz)* (IEEE, 2020), pp. 1–2.
50. L. Liebermeister, S. Nellen, R. B. Kohlhaas, S. Lauck, M. Deumer, S. Breuer, M. Schell, and B. Globisch, "Optoelectronic frequency-modulated continuous-wave terahertz spectroscopy with 4 THz bandwidth," Nat. Commun. **12**(1), 1071 (2021).

Optics EXPRESS


51. M. Deumer, S. Breuer, R. Kohlhaas, S. Nellen, L. Liebermeister, S. Lauck, M. Schell, and B. Globisch, "Continuous wave terahertz receivers with 4.5 THz bandwidth and 112 dB dynamic range," Opt. Express **29**(25), 41819–41826 (2021).
52. T. Kawanishi, "Thz and photonic seamless communications," J. Lightwave Technol. **37**(7), 1671–1679 (2019).
53. S. Koenig, J. Antes, D. Lopez-Diaz, I. Kallfass, T. Zwick, C. Koos, W. Freude, and J. Leuthold, "High-speed wireless bridge at 220 GHz connecting two fiber-optic links each spanning up to 20 km," in *Optical Fiber Communication Conference* (Optical Society of America, 2012), paper OM2B–1.
54. A. Kanno, P. T. Dat, N. Sekine, I. Hosako, N. Yamamoto, Y. Yoshida, K.-I. Kitayama, and T. Kawanishi, "Seamless fiber-wireless bridge in the millimeter-and terahertz-wave bands," J. Lightwave Technol. **34**(20), 4794–4801 (2016).
55. T. Li, L. Gonzalez-Guerrero, H. Shams, C. Renaud, A. J. Seeds, M. Fice, I. White, and R. Penty, "Novel compressed digital radio fronthaul over photonically-generated THz wireless bridge," in *Optical Fiber Communications Conference and Exhibition (OFC)* (IEEE, 2020), pp. 1–3.
56. S. Ummethala, T. Harter, K. Koehnle, Z. Li, S. Muehlbrandt, Y. Kutuvantavida, J. Kemal, P. Marin-Palomo, J. Schaefer, A. Tessmann, S. K. Garlapati, A. Bacher, L. Hahn, M. Walther, T. Zwick, S. Randel, W. Freude, and C. Koos, "Thz-to-optical conversion in wireless communications using an ultra-broadband plasmonic modulator," Nat. Photonics **13**(8), 519–524 (2019).
57. Y. Horst, T. Blatter, and L. Kulmer, *et al.*, "Transparent optical-thz-optical link at 240/192 gbit/s over 5/115 m enabled by plasmonics," J. Lightwave Technol. **40**(6), 1690–1697 (2022).